Search for nonextensivity in electron-proton interactions at $\sqrt{s} = 300$ GeV

Soumya Sarkar*
Indian Institute of Science Education and Research, Pune, India

R. Aggarwal†
USAR, Guru Gobind Singh Indraprastha University, East Delhi Campus 110092, India

M. Kaur‡
Department of Physics, Panjab University, Chandigarh 160014, India
and Department of Physics, Amity University, Punjab, Mohali 140306, India

(Received 28 September 2023; accepted 23 February 2024; published 25 March 2024)

Study of canonical entropy in electron-proton interactions at $\sqrt{s} = 300$ GeV is presented. The precision data collected by the H1 experiment at the HERA in different ranges of invariant hadronic mass W and the squared four-momentum exchange Q^2 in electron-proton (ep) interactions have been analyzed in the ensemble theory approach. The canonical partition function relates to the multiplicity distribution which is often studied in collider experiments. We use the canonical ensemble partition function to explore the dynamics of hadron production in ep interactions by devising different methods to find the entropic parameter and the collision temperature. The inverse slope of the transverse momentum spectrum of produced hadrons also relates to the temperature. In the recent past, the CMS, ATLAS, and ALICE experiments at the LHC have studied the charged hadron transverse momentum and particle distributions in proton-proton and proton-nucleus interactions by using the Tsallis function within this approach. A detailed investigation into the role of the system volume and relation amongst different dynamical parameters reveals interesting results.

DOI: 10.1103/PhysRevD.109.052008

I. INTRODUCTION

The application of ensemble theory of statistical mechanics to particle interactions gives interesting results to understand the interaction dynamics. High-energy collisions of subatomic particles such as pions, protons, electrons, and the heavy ions, etc. produced at the particle accelerators are studied systematically with high precision. The production of particles, both known and unknown in such collisions are also studied in terms of physics principles emerging from the ensemble theory. Many of the physical observables such as hadron multiplicity, rapidity and transverse momentum etc., which are few of the different outcomes from these collisions are understood by modeling through the concepts of thermodynamics and statistical mechanics [1–6]. Exciting new results from the estimated behavior of these observables as a function of center-of-mass energy have emanated from the detailed investigations allowing the predictions for the future experiments in pursuit of discovery of new particles [6–8]. Ensemble theory has been used in several studies of particle production. The multiplicity of particles produced in a collision and its relation with the thermodynamic temperature of a collision are used to access dynamics of the particle interactions. Visualizing a particle interaction as a microcanonical or canonical or grand-canonical ensemble is one of the interpretations which has led to the understanding of particle-production mechanisms. For example the canonical partition function relates to the multiplicity distribution often measured in collider experiments and the transverse momentum spectrum reveals information on the early thermal or close to thermal properties of the hot state of such collisions [8–11] etc.

Standard statistical mechanics of Boltzmann-Gibbs which treats entropy as an extensive property of the system and the models based on this have not been very satisfactory. The possible sources of deviations included intrinsic and nonstatistical effects, in particular fluctuations in the properties of entropy. A generalized form of the entropy was postulated by C. Tsallis introducing a redefinition [12] as follows.

*soumya.sarkar@students.iiserpune.ac.in
†ritu.aggarwal1@gmail.com
‡manjit@pu.ac.in

The standard expression for entropy is $S = -k\sum_{i=1}^{W} p_i \ln p_i$ where $W \in N$ is the total number of possible configurations corresponding to $\{p_i\}$ associated probabilities and $\sum_{i=1}^{W} p_i = 1$. The entropy S is thus an extensive property of any thermodynamical system. However, in the redefinition of entropy, $S_q = \frac{k}{q-1}\sum_{i=1}^{W} p_i(1 - p_i^{q-1})$, where k is a positive constant, $q > 1$ makes the entropy a nonextensive property of the system. The q, also known as the entropic index, characterizes the degree of nonextensivity and the additive entropy rule stands modified,

$$S_q(A + B) = [S_q(A)] + [S_q(B)] + (q - 1)[S_q(A)][S_q(B)], \tag{1}$$

where A and B are two independent systems and $q > 1$ is a measure of the nonextensivity of entropy. For $q = 1$, one recovers back the Boltzmann-Gibbs(BG) statistics.

Thermostatistics has been applied to describe the particle production in high-energy particle interactions. Predictions of a thermodynamical model of hadron production for multiplicity distributions in e^+e^- annihilation at LEP and PEP-PETRA energies have been used to establish a two-step process resulting into the clan structure [6,13–15]. The clan model was introduced in order to interpret the wide occurrence of the negative binomial regularity of charged particle multiplicity distribution in high-energy reactions [6,16]. In a reaction any produced particle originates from a primary particle (or a parton), named ancestor. All the particles with a common ancestor form a clan. The clans have no mutual interaction. The reaction dynamics may be such that all the produced particles may be correlated. Thermostatistical aspects play an important role in the investigations in high-energy collisions of two particles or heavy ions to predict and understand the form of statistical equilibrium. One of the signatures of "thermal" multiparticle production is the exponential form of the transverse energy distribution of the produced hadrons. The slope parameter of this distribution can be interpreted in terms of a temperature of the final state [8,17,18].

The slope of this distribution is interpreted in terms of a temperature of the final state. The particle multiplicities and transverse energy distribution are found to be consistent with such an interpretation, at lower energies. At higher energies, the thermal interpretation of the transverse energy spectra is modified and described well by the nonextensive thermostatistics of Tsallis [12,19,20]. At energies ($\sqrt{s} = 200$ GeV and beyond) in pp collisions a significant deviation from the exponential transverse energy distribution, together with the violation of Koba-Nielsen-Olesen (KNO) [21] scaling law was encountered.

The nonextensive generalization of the statistical mechanics has gained importance in describing the collisions at collider experiments. It has been extensively studied in different type of high-energy collisions [22–27] up to the highest energy data from e^+e^- collisions, pp collisions and for heavy-ion collisions [11,28–31]. Most of these studies have focused on the particle properties and in particular the charged particle multiplicities and the transverse momentum spectra [8,32–34]. In the recent past, the CMS, ATLAS, and ALICE experiments at the Large Hadron Collider (LHC) have studied the charged hadron transverse momentum distributions in proton-proton and proton-nucleus interactions by using the Tsallis function [12,35–37]. In addition to the description of the transverse energy spectra, the extended statistical approach to describe multiparticle production can be used to predict the temperature.

In this paper we present the first study in terms of canonical entropy from the multiplicities in different kinematic regions of electron-proton collisions at the Hadron-Electron-Ring Accelerator (HERA). The precision data of proton-proton interactions at the intersecting storage rings (ISR) at different energies have been analyzed for the validation. We use these two different methods to describe the properties of multiplicity distributions and their temperature dependence. Section II describes the concepts; the equations used for computing entropic index and the temperature with some inputs from [38]. Details of the data being analyzed are given in Sec. III. Methodology developed for determining the parameters are given in Sec. IV. Results and discussion are presented in Sec. V, followed by conclusions in Sec. VI.

II. MULTIPLICITY AND GENERALIZED CANONICAL PROBABILITY

An important observable in the particle interactions is the multiplicity distribution of the produced hadrons. One of the most popular ways of expressing the probability distribution of these hadrons is the negative binomial distribution [39,40], which is known to arise with some specific processes such as accompanying the Bose-Einstein particles with different sources. The following subsection outlines the distribution.

A. Negative binomial distribution

The multiplicity of particles produced in an interaction can be described in terms of the negative binomial distribution (NBD), which is the following probability law for multiplicity $n \geq 0$:

$$P_n = \frac{k(k+1).....(k+n-1)}{n!}\left(\frac{\langle n\rangle}{\langle n\rangle + k}\right)^n \left(\frac{k}{\langle n\rangle + k}\right)^k, \tag{2}$$

where $\langle n\rangle$ is the mean number of produced particles called the average multiplicity and $k > 0$ is related to the variance D of the distribution as

$$\frac{1}{k} = \frac{D^2 - \langle n\rangle^2}{\langle n\rangle}. \tag{3}$$

The negative binomial distribution has been extensively used to fit the multiplicity distributions by nearly all high-energy physics experiments. It is remarkably well-described the data at lower energies, but showed significant deviations at higher energies. The weighted combinations of NBDs have been used to improve its applicability [41–43].

B. The q-statistics

It is well-known that several features of particle production in high-energy hadronic collisions can be described by thermostatistical models. A phase of nuclear matter consisting of quarks and gluons in such collisions is expected to lead to some form of statistical equilibrium, subsequently leading to the formation of locally thermalized source of particles. The generalized statistical mechanics (with $q > 1$) affects the hadronic multiplicity distribution in such collisions. In usual thermostatistics the generalized entropy S is defined [38] by introducing the q-entropy,

$$S = \frac{1 - \sum_a P_a^q}{q - 1}, \tag{4}$$

$$\sum P_a = 1, \tag{5}$$

where P_a is the probability of microstate a with the total probability being normalized to unity. Any physical observable O in this approach has a q-biased average value defined as

$$\langle O \rangle = \frac{\sum_a O_a P_a^q}{\sum_a P_a^q}, \tag{6}$$

and the q-biased microstate probability,

$$\tilde{P}_a = \frac{P_a^q}{\sum_a P_a^q}, \tag{7}$$

is the probability to be used in calculation of physical quantities. In the limit, when the entropic index $q \to 1$, the normal Boltzmann-Gibbs-Shannon entropy is recovered [44]. The equilibrium probabilities P_a are determined by maximizing the entropy under the requisite constraints on the charge and energy conservation. For a fixed value of energy E, the conserved electric charge is Q. The constraints are implemented through the variational principle, using the method of undetermined Lagrange multipliers and using the normalization conditions on the energy E_a and charge Q_a of a microstate a. The variational principle gives,

$$\delta S + c_1 \sum_a \delta p_a - c_2 \delta E + c_3 \delta Q = 0, \tag{8}$$

where

$$E = \sum_a E_a \tilde{p}_a, \tag{9}$$

$$Q = \sum_a Q_a \tilde{p}_a, \tag{10}$$

where the constants c_1, c_2, and c_3 are Lagrange multipliers. The temperature T and chemical potential are related to c_2 and c_3 as

$$c_2 = \frac{1}{T} = \left(\frac{\partial S}{\partial E}\right)_{Q,V}, \tag{11}$$

$$c_3 = \frac{\mu}{T} = -\left(\frac{\partial S}{\partial Q}\right)_{E,V}. \tag{12}$$

The $\tilde{P}_a$ distribution can be obtained by solving the variational principle and is given as

$$\tilde{P}_a = \frac{(\exp_q[-\beta(E_a - \mu Q_a)])^q}{\sum_a (\exp_q[-\beta(E_a - \mu Q_a)])^q}. \tag{13}$$

The denominator in Eq. (13) is called the generalized partition function, $Z_q(\beta, \mu, V)$. The q-potential function, $\exp_q$ is defined by

$$\exp_q(A) = [1 - (q-1)A]^{-1/(q-1)}. \tag{14}$$

β is related to the temperature T by

$$T = \frac{\beta^{-1} + (q-1)(E - \mu Q)}{1 + (1-q)S}, \tag{15}$$

and when $q \sim 1$,

$$[\exp_q(A)]^q \sim \exp[A + (q-1)(A + A^2/2)]. \tag{16}$$

The Lagrange multipliers express the temperature and chemical potential. A characterization of thermal equilibrium connects the so called "physical" temperature via

$$\tilde{T} = \beta^{-1} + (q-1)(E - \mu Q). \tag{17}$$

Chemical potential μ controls the average charge Q in the grand canonical approach discussed. For small values of $Q(= 1)$, when fluctuations about the mean become significant, the canonical treatment is preferred and $\mu = 0$. The generalized partition function for fixed charge becomes,

$$Z_q(\beta, Q, V) = \sum_a \delta(Q - Q_a)(\exp_q[-\beta(E_a)])^q, \tag{18}$$

where $\delta(Q - Q_a)$ is the Kronecker delta. The generalized canonical probability is given as

$$\tilde{P}_a = \frac{\delta(Q - Q_a)}{Z_q(\beta, Q, V)} [\exp_q(-\beta(E_a)]^q. \tag{19}$$

The probability that a system has exactly N number of particles in the Tsallis statistics, with N_a particles in a given state a is

$$P_N = \sum_a \delta(N - N_a)\tilde{P}_a. \tag{20}$$

The N-particle partition function can then be written as

$$Z_q^{(N)}(\beta, \mu, V) = \sum_a \delta(N - N_a)[\exp_q(-\beta(E_a - \mu Q_a))]^q, \tag{21}$$

where

$$P_N = \frac{Z_q^{(N)}}{Z_q}. \tag{22}$$

The generating function for the multiplicity distribution can now be defined by

$$F(t) \equiv \sum_{N=0}^{\infty} t^N P_N. \tag{23}$$

The multiplicity distribution for the N-particle system can then derived from the generating function. For example, for the negative binomial distribution the generating function is

$$F_{\mathrm{NB}}(t) = \left[1 - \frac{\langle N\rangle}{k}(t-1)\right]^{-k} = \exp_q[\langle N\rangle(t-1)]. \tag{24}$$

With $q = 1 + 1/k$, Eq. (24) gives the negative binomial distribution. For large values of k or small values of q we have the asymptomatic behavior of $F_{\mathrm{NB}}(t)$ given by

$$F_{\mathrm{NB}}(t) \approx \exp\left[\langle N\rangle(t-1) + \frac{\langle N\rangle^2}{2k}(t-1)^2\right]. \tag{25}$$

When these results are applied to an ideal relativistic gas to study the Tsallis statistics of hadron gas, it is observed that with $q > 1$ the generalized partition function Z_q becomes infinite. Thus, there is no ideal Tsallis gas with $q > 1$ and the q-statistics of an ideal relativistic gas cannot be defined. However, the case $q > 1$ is the focus of interest in high-energy collisions. For an ensemble of N particles, the generalized ideal gas partition function $Z_q^{(N)}$ has a well-defined integral representation in terms of the corresponding Boltzmann-Gibbs function subject to the condition that $N < \frac{1}{3(q-1)}$. Particle production above this limit is the cause of divergence in the partition function of the Tsallis ideal gas. One way to include such interactions is to introduce a "Van der Waals" excluded volume simulating the effect of hard-core potentials among particles. It tries to model the effect of nonzero volume of particles of the system as opposed to ideal gas where the volume of particles are taken to be zero [45,46]. Also the ideal gas system is noninteracting but Van der Waals gas takes into account the interaction by considering the particles as hard spheres. The repulsive interactions among the produced particles are thus responsible for the divergence in partition function of the Tsallis ideal gas. To include such interactions, the Van der Waals excluded volume was introduced. This Van der Waals gas model has been used to study particle abundances in high-energy heavy-ion collisions as it gives an appropriate description of the particle dynamics in the gas. The Van der Waals gas model as well as the Boltzmann-Gibbs statistics with extensive entropy ($q = 1$) produce a multiplicity distribution with a narrower width as compared with the experimental distribution. However, with Tsallis statistics, increasing q very slightly ($q > 1$) a much broader distribution is obtained and in good agreement with the experimental data. This result is true for data at different energies.

C. Excluded volume for N-particle system

The ideal gas description proved to be inadequate in many ways. A primary reason being it does not consider the interaction and finite volume of its constituent particles. The simplest way to add an interaction and also a finite volume is to consider the repulsive hard-core or hard-sphere potential. In this case, the volume which remains inaccessible to other particles of the system as a result of the presence of the first particle, is called the excluded volume. For example, the excluded volume of a single hard sphere (particle) is eight times its volume. If the system has two identical hard spheres then the excluded volume gets distributed among the two [47]. Assuming that the two spheres are identical, it becomes four times the volume of each sphere, as shown in the schematic Fig. 1. For a hard-core sphere the excluded volume depends on the radius of the spheres. In principle all particles can have their own hard-core radii, subject to the restrictions that:

(i) $V_{ex} \ll V$, with V is the total volume of the system and V_{ex} the total excluded volume of all particles;
(ii) Also as described in Ref. [48], the radii should not be too small to circumvent any contradiction with lattice quantum chromodynamics (LQCD). This results in having certain flexibility in defining the value of excluded volume or hard-core radii as long as these conditions are satisfied. It has been observed that excluded volume remains nearly constant for nucleon-nucleon scattering. For nucleon-nucleon scattering this value of hard-core radius (r_0) is observed to be around $r_0 = 0.3$ fm[48]. For the current analysis we take the value of excluded volume, $v_0 = 0.368$ fm^3, same as used in [38] for all the analysis of pp interactions. We use the same value for analysis of ep interactions as well since for all-hadron final state a constant value of v_0 can be

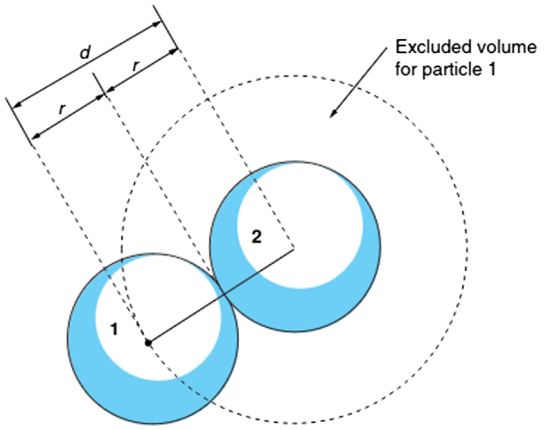

FIG. 1. Schematic figure of excluded volume with two hard spheres [47].

used, as mentioned earlier. To further understand the effect of Tsallis and Van der Waals corrections to the ideal gas, necessary details as described by Aguiar and Kodama in Ref. [38] are reproduced below.

The starting point is the relativistic ideal gas. For a relativistic ideal gas the Boltzmann-Gibbs grand canonical partition function is given by

$$Z(\beta,\mu,V)=\exp\left(V\sum_{i=1}^{h}\Phi_i(\beta)\exp(\beta\mu q_i)\right), \quad (26)$$

where

$$\Phi_i(\beta)=\frac{g_i}{2\pi^2}\frac{m_i^2}{\beta}K_2(\beta m_i), \quad (27)$$

g_i denotes the degeneracy factor of ith hadron species with mass m_i and charge q_i. h denotes the total number of hadrons. $K_2(z)$ is the modified Bessel function of second kind. β denotes the inverse temperature, μ denotes the chemical potential and V the volume of the system. Hence, the N-particle partition function is given by

$$Z^{(N)}(\beta,\mu,V)=\frac{1}{N!}\left(V\sum_{i=1}^{h}\Phi_i(\beta)\exp(\beta\mu q_i)\right)^N. \quad (28)$$

To have Van der Waals-type effects in relativistic gas an excluded volume v_0 is introduced, which changes V to $V-Nv_0$ to take into account the finite volume of particles. The partition function got modified as

$$Z^{(N)}(\beta,\mu,V)\to Z^{(N)}(\beta,\mu,V-Nv_0)\Theta(V-Nv_0). \quad (29)$$

The Heaviside Θ function limits the number of particles to be fitted in a particular volume V i.e., $N<V/v_0$. The partition function of a relativistic Van der Waal's gas is given by

$$Z(\beta,\mu,V)=\sum_N\frac{1}{N!}n(\beta,\mu)^N(V-Nv_0)^N\Theta(V-Nv_0). \quad (30)$$

Here $n(\beta,\mu)$ denotes the particle density and its expression can be derived from ideal relativistic gas,

$$n(\beta,\mu)=\sum_{i=1}^{h}\Phi_i(\beta)\exp(\beta\mu q_i). \quad (31)$$

In the large V asymptotic limit, partition function for relativistic ideal gas reduces to

$$Z(\beta,\mu,V)=\exp\left\{\frac{V}{v_0}W[v_0n(\beta,\mu)]\right\}, \quad (32)$$

where $W(x)$ is the Lambert function. Hence, from Eq. (32) the q-exponential partition function and hence generating function can be derived as

$$Z_q(\beta,\mu,V)=\int_0^\infty dxG(x)\exp\left\{\frac{V}{v_0}W[v_0n(x\beta,\mu)]\right\} \quad (33)$$

$$F(t)=\frac{1}{Z_q(\beta,\mu,V)}\int_0^\infty dxG(x)\exp\left\{\frac{V}{v_0}W[tv_0n(x\beta,\mu)]\right\} \quad (34)$$

The partition function Z_q then remains convergent as long as $q<1+\frac{v_0}{3V}$. To understand the effect of Tsallis statistics on the multiplicity distribution, the case in which $q-1$ and v_0 are both small, the generating function for the Van der Waals–Tsallis relativistic gas can be written as:

$$F(t)\approx\exp\Big\{(t-1)Vn[(1+(q-1)\xi(Vn\xi-1)-2v_0n] + (t-1)^2(Vn)^2\left[(q-1)\frac{\xi^2}{2}-v_0/V\right]\Big\}, \quad (35)$$

where ξ in Eq. (35) is given by

$$\xi=-\frac{\beta}{n}\frac{\partial n}{\partial\beta} \quad (36)$$

and $n\equiv n(\beta,\mu)$ is given by Eq. (31).On comparing Eq. (35) with generating function for negative binomial distribution, Eq. (25), the values of $\langle N\rangle$ and k can be deduced and is given by

$$\langle N\rangle=n_0+(q-1)n_0\xi(n_0\xi-1)-\frac{2v_0}{V}n_0^2, \quad (37)$$

$$\frac{1}{k}=(q-1)\xi^2-\frac{2v_0}{V}. \quad (38)$$

Where $n_0 \equiv Vn$ denotes the number of particles at a fixed temperature [n as defined by Eq. (31) and $\xi \equiv \xi(\beta,\mu) = -\frac{\beta}{n_0}\frac{\partial n_0}{\partial \beta}$ as given by Eq. (36)]. For further analysis, we take $\mu = 0$. Hence, n_0 is given by

$$n_0 = V\sum_{i=1}^{h}\Phi_i(\beta). \tag{39}$$

All the equations have been adopted from [38]. Using Eqs. (37) and (38) the temperature, β^{-1} and nonextensivity parameter, q can be derived, from experimental quantities namely average charged multiplicity, $\langle N\rangle$ and k, which are related to width and shape of the NBD distribution, as given in Eq. (3).

III. DATA USED

The primary aim of the analysis is to study the hadronic multiplicities in ep interactions at HERA energy using the canonical partition function with the q-statistics. This is the first analysis with this data. The analysis of data from pp interactions at ISR energies also has been done for the same reason, in addition to it being used for the purpose of validation. Beyond these energies, the KNO scaling [21] violations were reported as mentioned in Ref. [49]. A separate analysis of the pp data for $\sqrt{s} > 200$ GeV is under consideration.

A. Electron-proton collisions at HERA

The data used for the present analysis were collected with the H1 detector [50] at the HERA storage ring at DESY during the 1994 running period which recorded collisions of positrons, with an incident energy of 27.5 GeV, and protons with an energy of 820 GeV giving $\sqrt{s} = 300$ GeV. Multiplicity distributions measured in four different kinematic regions in $W = 80$–115 GeV, 115–150 GeV, 150–185 GeV, 185–220 GeV for charged particles and in four different pseudorapidity sectors; $1 < \eta^* < \eta_c^*$ with $\eta_c^* = 2,3,4,5$ have been analyzed.

1. Kinematics of deep inelastic scattering

In deep inelastic scattering, a high-energy lepton scatters off a hadron after interaction with one of its constituents through a virtual photon or a weak boson as shown in Fig. 2. Let the initial 4-momentum of lepton be k and final 4-momentum k'. The initial 4-momentum of proton be p, fraction of proton momentum carried by the struck quark as x and final 4-momentum of the hadronic system be p'. The following invariant variables can be defined:

$$s = (p+k)^2, \tag{40}$$

$$t = (p-p')^2, \tag{41}$$

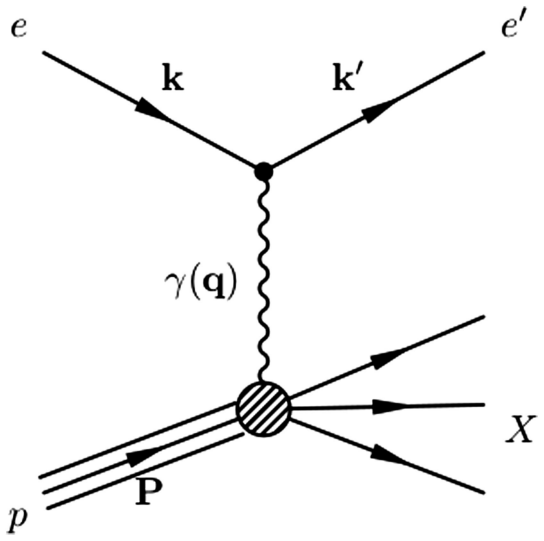

FIG. 2. Deep inelastic scattering of lepton on hadron.

$$Q^2 = -q_\gamma^2 = -(k-k')^2, \tag{42}$$

$$y = \frac{p.q_\gamma}{p.k'}, \tag{43}$$

$$W^2 = (p')^2 = (p+q_\gamma)^2. \tag{44}$$

Where s is the center-of-mass energy squared, t is the four-momentum transferred squared between proton and final-state hadronic system, Q^2 is negative square of the four-momentum transferred (q_γ) from the electron to the proton, y is the inelasticity of the scattered lepton, and W^2 is the invariant squared mass of final state hadrons. The energy-momentum conservation demands that,

$$x = \frac{Q^2}{2p.q_\gamma}, \tag{45}$$

$$y = \frac{Q^2}{sx}, \tag{46}$$

$$W^2 = Q^2\frac{1-x}{x}. \tag{47}$$

Pseudorapidity is defined as $\eta^* = -\ln\tan\frac{\theta}{2}$, with θ the angle between the hadron momentum and the direction of the virtual photon in the $\gamma^* p$ rest system.

B. Proton-proton collisions at the ISR

The second dataset used was obtained by the experiment at the CERN ISR using the SFM detector to measure momenta of all charged particles. Four samples of non-single-diffractive (NSD) events were obtained from the pp collisions at $\sqrt{s} = 30.4$ GeV, 44.5 GeV, 52.6 GeV, and

62.2 GeV. The experiment, data samples and event selection procedure are given in [51,52].

IV. METHODOLOGY

In the present analysis, we study the particle multiplicity distributions aiming to understand the effect of q-statistics. The selected data are being analyzed using the Tsallis statistics to search for the nonextensive behavior of these interactions as described in Sec. II. Following the details provided in the section, we devise two different methods, as described below, to solve for the nonextensivity parameter q and temperature, β^{-1}.

A. Method 1

In this method the ξ dependence on β is studied and the value of β is obtained as follows. We rearrange Eq. (38) to obtain $(q-1)$ given in Eq. (48),

$$(q-1) = \frac{1/k + 2v_0/V}{\xi^2}, \tag{48}$$

and substituting $(q-1)$ into Eq. (37), we get the following expression for ξ:

$$\xi = \frac{\alpha_1 n_0}{n_0 + (\alpha_1 - \alpha_2)n_0^2 - \langle N\rangle}, \tag{49}$$

$$\text{where } \alpha_1 = \frac{1}{k} + \frac{2v_0}{V}, \tag{50}$$

$$\alpha_2 = \frac{2v_0}{V}. \tag{51}$$

Using Eqs. (39) and (27), n_0 can be obtained as a function of β, and putting this value of n_0 in Eq. (49), ξ can be obtained as a function of β.

The expression of ξ can also be deduced from Eqs. (39), (27), and (36) which is based on theoretical Tsallis model and does not use the $\langle N\rangle$ and k as used above. The steps are outlined as follows:

$$\xi = -\frac{\beta}{n_0}\frac{\partial n_0}{\partial \beta}, \tag{52}$$

$$\Phi_i(\beta) = \frac{g_i m_i^2}{2\pi^2 \beta} K_2(\beta m_i), \tag{53}$$

where n_0 is given by Eq. (39) as follows:

$$n_0 = V\sum_{i=1}^{h} \Phi_i(\beta). \tag{54}$$

$K_n(z)$ below refers to modified bessel function of second kind. putting $n = 2$ gives us an expression to calculate ξ as given below,

$$\frac{\partial K_n(z)}{\partial z} = -K_{n-1}(z) - \frac{n}{z}K_n(z), \tag{55}$$

$$\frac{\partial K_2(\beta m)}{\partial \beta} = -mK_1(\beta m) - \frac{2}{\beta}K_2(\beta m), \tag{56}$$

$$\frac{\partial \Phi_i(\beta)}{\partial \beta} = \frac{g_i m_i^2}{2\pi^2}\left[-\frac{K_2(\beta m_i)}{\beta^2} - \frac{1}{\beta}\left(m_i K_1(\beta m_i) + \frac{2}{\beta}K_2(\beta m_i)\right)\right]. \tag{57}$$

Finally we get ξ as

$$\xi = \frac{1}{\Sigma m_i^2 g_i K_2(\beta m_i)}\Sigma m_i^2 g_i [3K_2(\beta m_i) + (\beta m_i)K_1(\beta m_i)]. \tag{58}$$

Both these expressions of ξ given by Eqs. (58) and (49) are solved simultaneously using a graphical method. Hence, plotting Eqs. (58) and (49) as a function of β, the point of intersection of the two plots gives the value of (β, ξ). The value of ξ is substituted in Eq. (48) to get the value of q.

The parameters $\langle N\rangle$ and k that go into the Eqs. (49) and (50) above are obtained by fitting a negative binomial distribution to the charged multiplicity distribution. We use the data for pp collisions at $\sqrt{s} = 44.5$ GeV data from Ref. [53] for validation with results from C. Aguiar *et al.* [38]. The fit procedure uses CERN ROOT6.2 library. The values of $\langle N\rangle = 12.21$ and $k = 9.226$ thus obtained are given in Table I. Using these values, Fig. 3 shows the plot of ξ versus β calculated both for Eq. (49) and for Eq. (58). Other values used for the calculations are from Ref. [38] as listed below:

(i) Excluded volume, $v_0 = 0.368$ fm^3 and Volume, $V = 40.1$ fm^3 are used from [38];

(ii) As described in Ref. [38], $\pi^{\pm,0}$, η, ω and $\rho^{\pm,0}$ are considered as the final-state hadrons, their mass and degeneracy factor are $m_\pi = 139.5$ MeV, $m_\eta = 548.8$ MeV, $m_\rho = 770$ MeV, and $m_\omega = 782$ MeV and $g_\pi = 3$, $g_\rho = 3$, $g_\eta = 1$, and $g_\omega = 1$.

The two curves in Fig. 3 intersect at $\beta \approx 0.00615$ MeV^{-1} which gives $\beta^{-1} \approx 162.60$ MeV. These results are in agreement with the values reported by Aguiar *et al.* in Ref. [38]. Method 1 therefore validates the correctness of our

TABLE I. Experimental $\langle N\rangle$ and fit parameters for NBD and χ^2/d.o.f for pp interactions at the ISR energies.

$\sqrt{s}$ (GeV)	$\langle N\rangle$ (Expt)	$\langle N\rangle$ (Fit)	k	χ^2/ndf
30.4	10.54 ± 0.14	10.73 ± 0.13	11.14 ± 0.69	24.04/15
44.5	12.08 ± 0.13	12.21 ± 0.11	9.23 ± 0.49	11.74/17
52.6	12.76 ± 0.14	12.79 ± 0.10	7.90 ± 0.28	7.93/19
62.2	13.63 ± 0.16	13.65 ± 0.14	8.35 ± 0.37	26.32/17

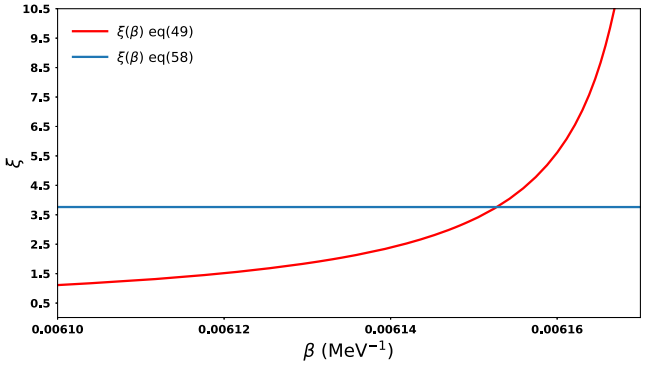

FIG. 3. ξ versus β for Eqs. (49) and (58) computed for pp collisions at $\sqrt{s} = 44.5$ GeV.

procedure to calculate the entropic index q and the temperature parameter, β^{-1}.

B. Method 2

In the second method, to solve for q and β we explicitly solve Eqs. (37) and (38). Rearranging these equations, we get the following set of equations:

$$n_0 + (q-1)n_0\xi(n_0\xi - 1) - \frac{2v_0}{V}n_0^2 - \langle N\rangle \equiv e_1, \quad (59)$$

$$(q-1)\xi^2 - \frac{2v_0}{V} - \frac{1}{k} \equiv e_2. \quad (60)$$

Substituting ξ from Eq. (58) into Eqs. (59) and (60), the equations are in terms of β and q. For a particular (β, q) when $e_1 \simeq 0$ and $e_2 \simeq 0$, that value of (β, q) is the desired solution. The values of parameters and constants used are the same as used in Method 1. A nonlinear solver *scipy.optimize.fsolve()* (a PYTHON module Ref. [54]) is used for solving the equations. By applying this method, we obtain the following values: $e_1 = -4.336 \times 10^{-12}$ and $e_2 \approx -6.522 \times 10^{-16}$, $\beta \approx 0.00615$ and $q \approx 1.0089$.

These values of the (β, q) pair which satisfy the equations, are consistent with the values obtained in Method 1 and also with the values quoted in Ref. [38]. Hence, it is confirmed that these methods indeed are the correct approach to solve for β and q. Having established the correctness of both methods, we use Method 2 for the analysis presented in this paper. Since Method 1 and Method 2 give exactly the same solution for β and q values, the choice does not affect the results.

V. RESULTS AND DISCUSSION

A. Charged multiplicities

As described in the two methods, the values of q and β^{-1} are validated with the results published in [38] for pp collisions for the 44.5 GeV data from ISR [51]. As further cross checks, we analyzed four sets of data from ISR range of energies by propagating experimental errors. The negative binomial distribution is fitted to the pp data at $\sqrt{s} = 30.4$ GeV, 52.6 GeV, 62.2 GeV. Table I gives the experimental value of average multiplicity and the NBD fit parameters. Table II shows the results for q and β^{-1} evaluated by using Method 2. The variation of q and β^{-1} with center-of-mass energy $\sqrt{s}$ is presented in Fig. 4. It is observed that q increases slowly and linearly with center-of-mass energy $\sqrt{s}$ as $q = a\sqrt{s} + b$ where $a = 7.4849 \times 10^{-5}$ and $b = 1.0055$. The parameter β^{-1} also increases linearly with the center-of-mass energy as $\beta^{-1} = c\sqrt{s} + d$ with $c = 0.09$ and $d = 157.65$.

TABLE II. q and β^{-1} values obtained from the pp interactions at different ISR energies [53].

$\sqrt{s}$ (GeV)	q	β^{-1} (MeV)
30.4	1.0076 ± 0.0004	160.81 ± 1.11
44.5	1.0089 ± 0.0005	162.47 ± 0.97
52.6	1.0102 ± 0.0004	161.80 ± 0.71
62.2	1.0097 ± 0.0004	164.46 ± 0.92

It is observed from Table II that the variations in q and β^{-1} values on account of quoted experimental errors are very small. Hence, for further analysis, the error values are not quoted.

Charged multiplicities in ep interactions in different W ranges obtained by the H1 [55] experiment at HERA, are analyzed using the canonical partition function and the

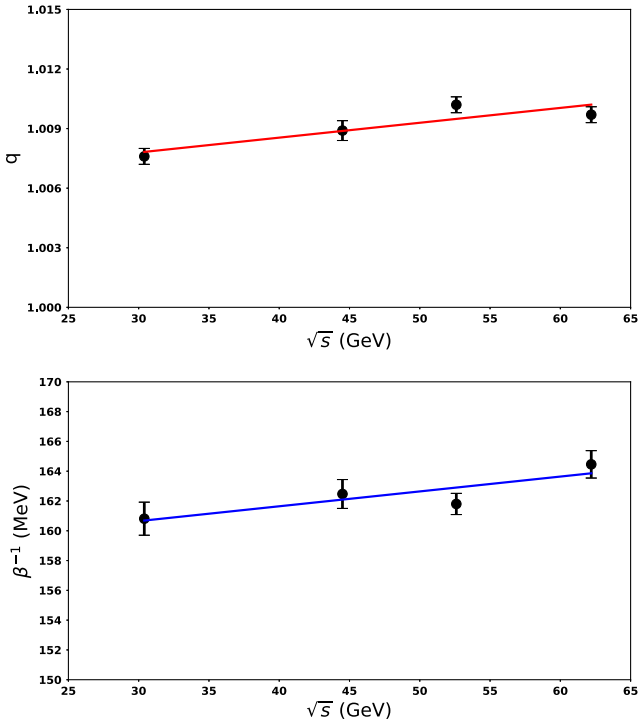

FIG. 4. variation of q (top) and β^{-1} (bottom) with $\sqrt{s}$ for pp collisions at the ISR energies [53].

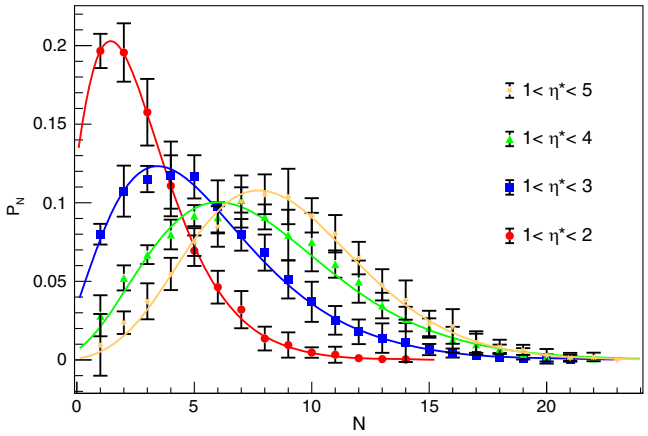

FIG. 5. NBD fit to the charged particle probability distribution in DIS of ep for $185 < W < 220$ GeV in the different pseudorapidity η^* sectors.

q-statistics. Values of entropic index q and the temperature are calculated. The data in four W ranges; 80–115 GeV, 115–150 GeV, 150–185 GeV, and 185–220 GeV and each range having data measured in four pseudorapidity intervals are analyzed. Thus a total of 16 datasets have been analyzed. To begin, each data is fitted with negative binomial distribution. Figure 5 shows the best-fit results for one energy range, $185 < W < 220$ GeV and four pseudorapidity sectors. Figures are given only for one invariant hadron-mass range W to avoid repetition of multiple similar diagrams. Table III shows the fit results for all the data. The χ^2/d.o.f. in Table III shows the accuracy of fitting. q and β^{-1} values calculated by using $v_0 = 0.368$ fm^3 and $V = 40.1$ fm^3 are shown in Table IV. Next we analyze both the ep and pp data in detail to study the relationships among various parameters. In a previous study [38] the q-statistics was studied in pp interactions by using V values between 24.5–49.2 fm^3 to reproduce the experimental multiplicity distributions. It is interesting to study the variation of β^{-1} and q as a function the volume V.

B. Variation of β^{-1} with V

Figure 6 shows a plot of β^{-1} as a function of volume V for ep collisions in one pseudorapidity sector, $1 < \eta^* < 2$ for W = 80–115 GeV, 185–220 GeV ranges, corresponding to the lowest and the highest $\langle W \rangle$ values. Similar distributions are studied for all W-ranges and of η^*-pseudorapidity sectors. Figures are not included to omit repetition. It is observed that the temperature (β^{-1}) decreases slowly with the increase in the volume for all ranges of W. We also studied the variation of β^{-1} for the different values of volume $V = 30$–75 fm^3 in four pseudorapidity sectors for the lowest and the highest $\langle W \rangle$ values. It is again observed that, β^{-1} decreases with volume V. With the increase in volume of the system, the temperature decreases by ≃25% as the volume changes from 30 fm^3 to 75 fm^3 for every $\langle Q^2 \rangle$. However, at a given value of V the temperature increases with $\langle Q^2 \rangle$. Figure 7 shows the dependence β^{-1} on V for pp collisions at different cms energies. It is observed that for pp interactions, β^{-1} falls with volume V i.e., with the increase in volume of the system, the temperature decreases for each center-of-mass energy. However, at a fixed value of the volume, the temperature rises with $\sqrt{s}$. From the p_T spectrum study using the Tsallis function, the results from the CMS experiment [35] also show that $T(\beta^{-1})$ increases with $\sqrt{s}$. Thus, the temperature dependence on volume is very similar in both type of interactions, ep and pp.

TABLE III. NBD fit parameters from Eq. (2) for the Charged particle multiplicity distributions in ep interactions. The data are obtained by the H1 experiment [55].

W range (GeV)	$\langle W \rangle$ (GeV)	η^*	$\langle Q^2 \rangle$ (GeV^2)	$\langle N \rangle$ (Expt)	$\langle N \rangle$ (Fit)	k	χ^2/ndf
80–115	96.9	$1 < \eta^* < 2$	13.9	2.46 ± 0.10	2.44 ± 0.11	3.09 ± 0.72	0.47/11
		$1 < \eta^* < 3$	27.6	4.90 ± 0.18	4.87 ± 0.14	4.71 ± 0.63	1.90/15
		$1 < \eta^* < 4$	55.0	6.45 ± 0.33	6.47 ± 0.17	9.78 ± 2.02	0.46/16
		$1 < \eta^* < 5$	385.3	6.90 ± 0.34	6.87 ± 0.14	15.91 ± 3.39	0.55/16
115–150	132.0	$1 < \eta^* < 2$	13.9	2.50 ± 0.12	2.54 ± 0.07	3.24 ± 0.44	0.60/12
		$1 < \eta^* < 3$	27.5	5.06 ± 0.27	5.10 ± 0.14	3.85 ± 0.46	1.79/16
		$1 < \eta^* < 4$	55.1	7.00 ± 0.35	7.07 ± 0.13	7.99 ± 0.89	3.51/18
		$1 < \eta^* < 5$	372.8	7.72 ± 0.42	7.68 ± 0.12	15.31 ± 2.30	3.75/19
150–185	166.8	$1 < \eta^* < 2$	13.9	2.63 ± 0.18	2.70 ± 0.09	3.77 ± 0.81	1.02/12
		$1 < \eta^* < 3$	27.6	5.32 ± 0.35	5.37 ± 0.13	3.85 ± 0.46	2.21/18
		$1 < \eta^* < 4$	55.1	7.51 ± 0.51	7.59 ± 0.19	7.43 ± 1.21	2.95/20
		$1 < \eta^* < 5$	378.4	8.45 ± 0.58	8.46 ± 0.20	12.23 ± 2.65	1.41/20
185–220	201.9	$1 < \eta^* < 2$	13.9	2.66 ± 0.18	2.71 ± 0.10	3.62 ± 0.78	0.49/12
		$1 < \eta^* < 3$	27.6	5.35 ± 0.35	5.38 ± 0.16	3.77 ± 0.43	1.87/19
		$1 < \eta^* < 4$	54.9	7.66 ± 0.47	7.76 ± 0.16	6.34 ± 0.73	6.00/20
		$1 < \eta^* < 5$	374.2	8.81 ± 0.55	8.83 ± 0.18	15.40 ± 2.93	4.22/21

TABLE IV. Values of q and β^{-1} for the ep interactions from the data obtained by the H1 [55] experiment in different W ranges.

W range (GeV)	$\langle W \rangle$ (GeV)	η^*	$\langle Q^2 \rangle$ (GeV^2)	q	β^{-1}
80–115	96.9	$1 < \eta^* < 2$	13.9	1.0228	111.37
		$1 < \eta^* < 3$	27.6	1.0152	130.92
		$1 < \eta^* < 4$	55.0	1.0080	144.76
		$1 < \eta^* < 5$	385.3	1.0057	150.17
115–150	132.0	$1 < \eta^* < 2$	13.9	1.0243	111.22
		$1 < \eta^* < 3$	27.5	1.0187	129.64
		$1 < \eta^* < 4$	55.1	1.0096	145.28
		$1 < \eta^* < 5$	372.8	1.0063	152.90
150–185	166.8	$1 < \eta^* < 2$	13.9	1.0243	112.34
		$1 < \eta^* < 3$	27.6	1.0197	130.22
		$1 < \eta^* < 4$	55.1	1.0112	145.45
		$1 < \eta^* < 5$	378.4	1.0069	154.52
185–220	201.9	$1 < \eta^* < 2$	13.9	1.0239	112.70
		$1 < \eta^* < 3$	27.6	1.0193	130.59
		$1 < \eta^* < 4$	54.9	1.0119	145.27
		$1 < \eta^* < 5$	374.2	1.0068	156.01

C. Variation of q with V

Figure 8 shows the variation of $(q-1)$ with volume V for ep collisions in $W = 80$–115 GeV and $W = 185$–220 GeV range and with different $\langle Q^2 \rangle$ values having pseudorapidity in $1 < \eta^* < 2$ interval. It is observed that q has nearly no dependence on V for each $\langle Q^2 \rangle$ value in the mentioned pseudorapidity region. Same trend is found in all pseudorapidity regions and W ranges. The $(q-1)$ decreases marginally with the increase in $\langle Q^2 \rangle$ for every V. However, $(q-1) > 0$ is always true which shows canonical entropy characteristically nonextensive.

Figure 9 shows the $(q-1)$ variation with V for pp collisions at different center-of-mass energies. Similar to the case of ep interactions, $(q-1)$ for each $\sqrt{s}$ is nearly constant for all V. Similar trend persists for all center-of-mass energies. However, q is always greater than unity at every V and every $\sqrt{s}$. The $(q-1)$ value increases with the center-of-mass energy $\sqrt{s}$. Thus, as the center-of-mass

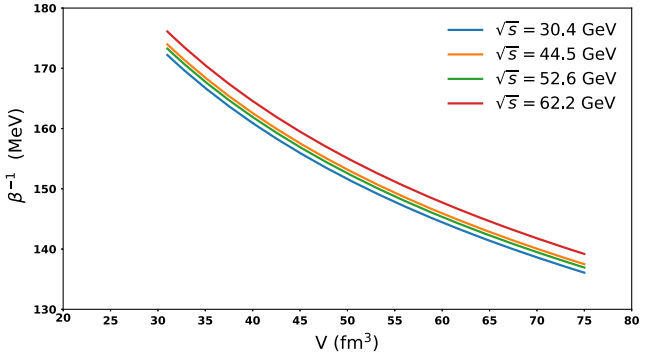

FIG. 7. β^{-1} versus volume V computed for pp collisions at four $\sqrt{s} = 30.5$ GeV, 44.5 GeV, 52.6 GeV, 62.2 GeV.

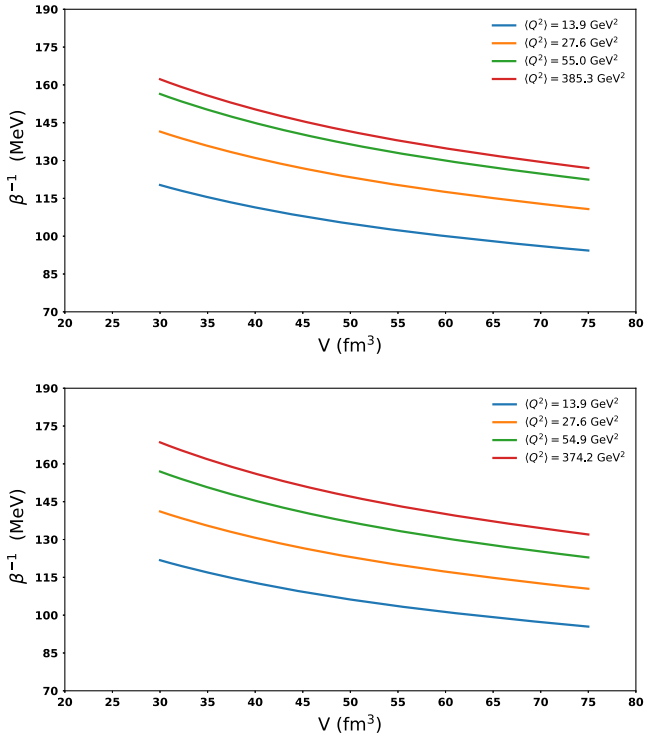

FIG. 6. β^{-1} versus volume V computed for ep collisions in the $W = 80$–115 GeV (top) and $W = 185$–220 GeV (bottom) range for the four values of $\langle Q^2 \rangle$.

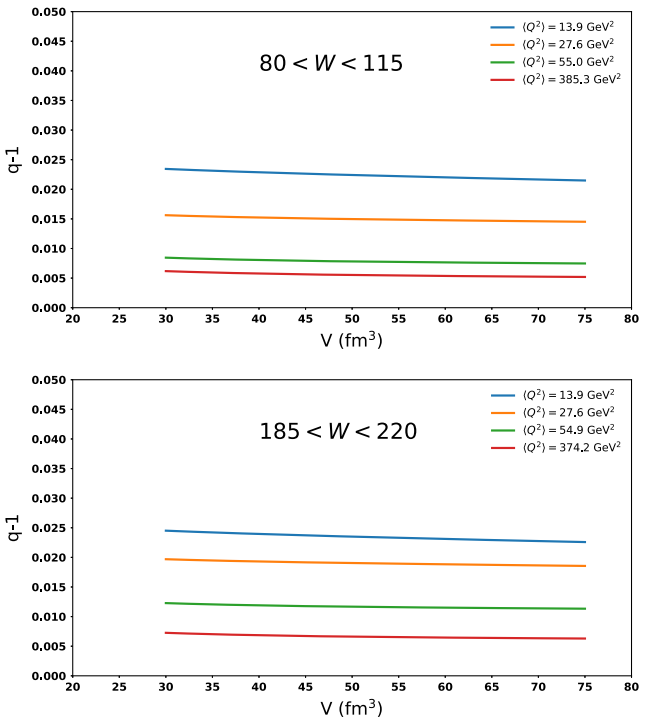

FIG. 8. $(q-1)$ versus V dependence for ep collisions in $W = 80$–115 GeV (top) and $W = 185$–220 GeV (bottom) range and with different $\langle Q^2 \rangle$.

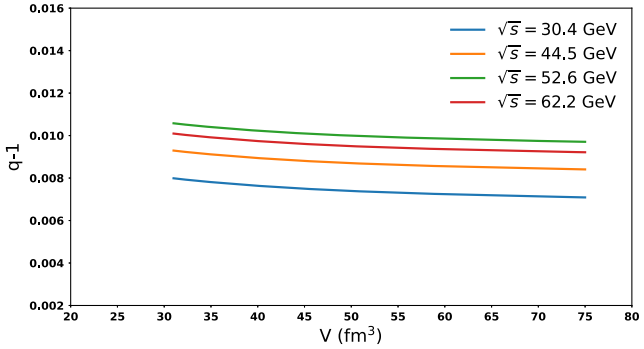

FIG. 9. Variation of $(q-1)$ with V for pp collisions at different energies.

energy of interaction increases, the nonextensive behavior of the system becomes more predominant.

D. Variation of q and β^{-1} with $\langle W\rangle$

To study the dependence of the entropic index q on the hadronic mass W, we show in Fig. 10 the variation plot for ep interactions in different η^* sectors. It is observed that q varies slightly but almost linearly with $\langle W\rangle$ in each phase-space region shown by the pseudorapidity range. The fit parameters of the linear fit are given in Table V. β^{-1} also depends linearly on $\langle W\rangle$ with a marginal change. However,

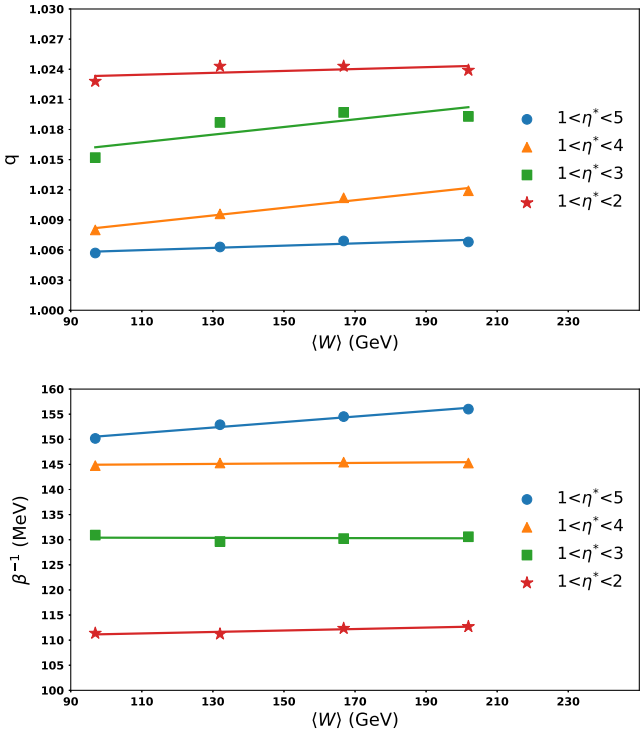

FIG. 10. Variations of q and β^{-1} versus $\langle W\rangle$ for ep interactions. $\langle W\rangle = 96.9$ GeV, 132.0 GeV, 166.8 GeV, 201.9 GeV corresponding to the W range 80–115 GeV, 115–150 GeV, 150–185 GeV, and 185–220 GeV, respectively.

TABLE V. Linear variation plot $q = a\langle W\rangle + b$ for ep interactions in different η^* sectors, from Table IV.

η^*	a $(\times 10^{-5})$	b
$1 < \eta^* < 5$	1.115	1.0047
$1 < \eta^* < 4$	3.802	1.0044
$1 < \eta^* < 3$	3.803	1.0125
$1 < \eta^* < 2$	0.939	1.0224

TABLE VI. Linear variation plot $\beta^{-1} = a\langle W\rangle + \mathrm{b}$ for ep interactions in different η^* sectors, from Table IV.

η^*	a $(\times 10^{-4})$	b
$1 < \eta^* < 5$	547	145.225
$1 < \eta^* < 4$	48	144.464
$1 < \eta^* < 3$	−12	130.519
$1 < \eta^* < 2$	145	109.727

both q and β^{-1} depend upon the phase-space size. While q decreases, β^{-1} increases with increasing η^* region. The linear fit is parameters are given in Table VI.

E. Variation of q and β^{-1} with $\langle Q^2\rangle$

The variations of q and β^{-1} as a function of $\langle Q^2\rangle$, the negative square of the four-momentum transferred from the electron to the proton, are shown in Fig. 11. The variation

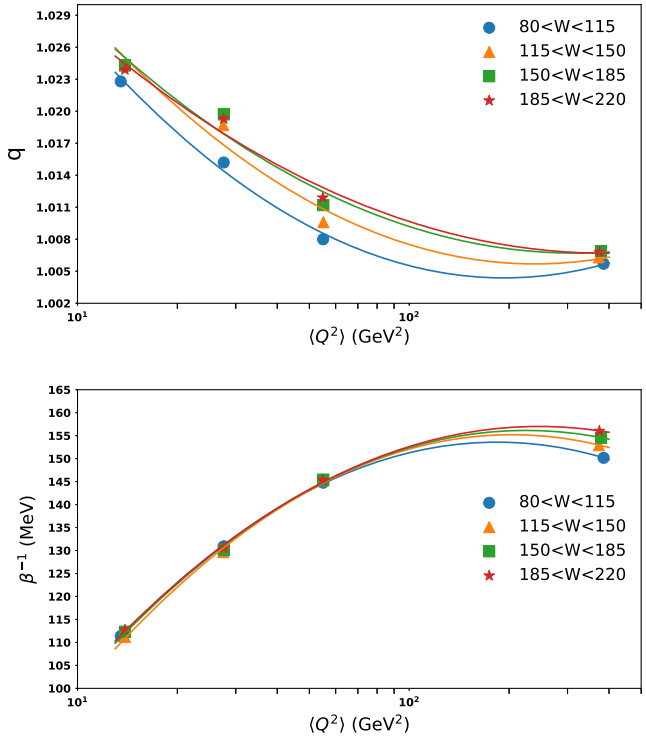

FIG. 11. q and β^{-1} versus $\langle Q^2\rangle$ variation for all ep interactions in different $\langle W\rangle$ values listed in the Table IV.

TABLE VII. Variation plot $q = a\log^2\langle Q^2\rangle - b\log\langle Q^2\rangle + c$ for ep interactions in different W ranges.

W (GeV)	a ($\times 10^{-4}$)	b($\times 10^{-4}$)	c
$80 < W < 115$	140	641	1.0776
$115 < W < 150$	126	602	1.0773
$150 < W < 185$	99	497	1.0688
$185 < W < 220$	84	438	1.0634

TABLE VIII. Plot $\beta^{-1} = -a'\log^2\langle Q^2\rangle + b'\log\langle Q^2\rangle - c'$ for ep interactions in different W ranges.

W (GeV)	a'	b'	c'
$80 < W < 115$	32.89	148.99	15.14
$115 < W < 150$	32.58	150.52	18.61
$150 < W < 185$	30.21	142.09	10.94
$185 < W < 220$	28.59	136.73	06.47

of q has a quadratic dependence on $\log\langle Q^2\rangle$ with parameters given in Table VII.

It may be observed that the q decreases quadratically with $\log\langle Q^2\rangle$. For a given $\langle Q^2\rangle$ the q value is higher for the interactions from higher W range i.e., higher $\langle W\rangle$. However for all values of $\langle Q^2\rangle$ the q remains greater than unity (> 1). This indicates the nonextensive dynamics of interactions.

On the other hand, temperature β^{-1} rises quadratically with $\log\langle Q^2\rangle$. The parameters of fit are given in Table VIII. Also at the highest $\langle Q^2\rangle$ value, the temperature is the highest for maximum $\langle W\rangle$. For a given $\langle W\rangle$ four-momentum transferred from the electron to the proton in an ep interaction increases with the phase space size i.e., from $|\Delta\eta^*| = 1$ to 4. Correspondingly the increase in the energy in the region results in increase in temperature.

VI. CONCLUSION

The paper presents the first analysis of ep interactions at $\sqrt{s} = 300$ GeV and pp interactions at various ISR energies by using the canonical partition function and q-statistics. We devised two different methods for finding the entropic parameter q and the temperature parameter β^{-1}. The two methods are validated with the previously published results [38] and are found to be consistent. The analysis of ep interactions in different ranges of the invariant mass of the hadronic system shows that the interactions deviate from Maxwell-Boltzmann statistics and show that the canonical entropy is nonextensive. The entropic parameter $q > 1$ for all W ranges and in all pseudorapidity sectors between $\eta^* = 1$ to 5. Similarly the analysis of pp interactions establishes that entropic parameter $q > 1$ for all center-of-mass energies. From a detailed study of the interdependence of $q, \beta, V, \sqrt{s}, \langle W\rangle$, and $\langle Q^2\rangle$, we observe that for ep interactions, with the increase in volume of the system, the temperature decreases at a given $\langle Q^2\rangle$. However, for fixed volume V, the temperature rises with $\langle Q^2\rangle$. The temperature dependence on volume is very similar in ep and pp interactions as observed from Figs. 6 and 7. It is observed that q has nearly no dependence on system volume for both ep and pp interactions. However, $q > 1$ is always true, which shows that the canonical entropy is characteristically nonextensive.

In ep interactions, q has a linear dependence on $\langle W\rangle$ and the value of q decreases with the increase in allowed phase space i.e., as the size of η^* sector increases. The temperature parameter β^{-1} depends marginally upon hadronic invariant mass $\langle W\rangle$ but β^{-1} increases with the size of the phase space, roughly from 111 MeV to 155 MeV as the η^* changes from $1 < \eta^* < 2$ to $1 < \eta^* < 5$. For a given $\langle W\rangle$, square of the four-momentum transferred from the electron to the proton $\langle Q^2\rangle$ in an ep interaction increases with the phase space size ($|\Delta\eta^*|$) as can be observed from Table IV. Correspondingly the temperature (β^{-1}) also increases. In the case of pp interactions q has linear dependence on $\sqrt{s}$, similar to the ep case. The temperature increases with the center-of-mass energy, $\sqrt{s}$. The results from the CMS experiment [35,36] have also shown that the temperature increases with the energy, $\sqrt{s}$.

It is concluded that canonical entropy derived in both ep and pp interactions is nonextensive, with entropic parameter $q > 1$. In the Van der Waals gas model with $q = 1$, the multiplicity distribution is narrower in width and does not agree with the data [38]. The Tsallis q-statistics broadens the width and reproduces the multiplicity distribution well. This also implies an increase in the events with higher multiplicity. In the limit of small $(q - 1)$, the distributions are well represented by negative binomial distribution. The present work has a potential scope of extension to the ep and electron-nucleus collisions at the future Electron-Ion Collider (EIC) and to pp and proton-nucleus collisions at the high luminosity (HL)-LHC experiments. The present study is validated using the pp collisions data at ISR energies and the entropic parameter is found to increase slightly with the energy, $\sqrt{s}$. The HL-LHC experiments will facilitate to explore the nature of entropic parameter and study the temperature parameter, β^{-1}, at higher $\sqrt{s}$ energies. The entropic parameter based on present study can be predicted to be nonextensive for pp collisions at higher energies. The future planned experiments at the EIC will enable to explore the nonextensive nature of entropic parameter, and temperature β^{-1} in ep collisions, at lower values of hadronic invariant mass $\langle W\rangle$ as compared to the present study.

ACKNOWLEDGMENTS

Author Soumya Sarkar acknowledges the support from the Department of Science and Technology, Govt. of India for the DST Inspire fellowship.

[1] T. Kanki, K. Kinoshita, H. Sumiyoshi, and F. Takagi, Prog. Theor. Phys. Suppl. **97**, 1 (1989).
[2] E. Kittel and E. De Wolf, *Soft Multihadron Dynamics* (World Scientific Publishing Company, Singapore, 2005).
[3] C. Tsallis, R. Mendes, and A. Plastino, Physica (Amsterdam) **261A**, 534 (1998).
[4] I. Dremin and J. Gary, Phys. Rep. **349**, 301 (2001).
[5] R. Ellis, *Entropy, Large Deviations, and Statistical Mechanics*, Grundlehren der mathematischen Wissenschaften (Springer-Verlag, Berlin, 1985).
[6] A. Giovannini and R. Ugoccioni, J. Phys. Conf. Ser. **5**, 190 (2005).
[7] G. G. Barnafoldi, K. Ürmössy, and T. S. Biró, J. Phys. Conf. Ser. **270**, 012008 (2011).
[8] L. Marques, J. Cleymans, and A. Deppman, Phys. Rev. D **91**, 054025 (2015).
[9] K. Kashiwa and H. Kouno, Phys. Rev. D **105**, 054017 (2022).
[10] K. Shen, G. G. Barnaföldi, and T. S. Biró, Eur. Phys. J. A **55**, 126 (2019).
[11] T. Wibig, J. Phys. G **37**, 115009 (2010).
[12] C. Tsallis, J. Stat. Phys. **52**, 479 (1988).
[13] F. Becattini, Z. Phys. C **69**, 485 (1995).
[14] F. Becattini, A. Giovannini, and S. Lupia, Z. Phys. C **72**, 491 (1996).
[15] A. Giovannini, *The Legacy of Leon Van Hove* (World Scientific, Singapore, 2000).
[16] A. Giovannini and L. Van Hove, Z. Phys. C **30**, 391 (1986).
[17] G. G. Barnaföldi, K. Ürmössy, and G. Bíró, J. Phys. Conf. Ser. **612**, 012048 (2015).
[18] L. Bianchini, R.-F. Si, H.-L. Li, and F.-H. Liu, Adv. High Energy Phys. **2018**, 7895967 (2018).
[19] I. Bediaga, E. Curado, and J. de Miranda, Physica (Amsterdam) **286A**, 156 (2000).
[20] C. Beck, Physica (Amsterdam) **286A**, 164 (2000).
[21] Z. Koba, H. B. Nielsen, and P. Olesen, Nucl. Phys. **B40**, 317 (1972).
[22] F. I. M. Pereira, R. Silva, and J. S. Alcaniz, Phys. Rev. C **76**, 015201 (2007).
[23] F. Pereira, R. Silva, and J. Alcaniz, Phys. Lett. A **373**, 4214 (2009).
[24] J. Conroy, H. Miller, and A. Plastino, Phys. Lett. A **374**, 4581 (2010).
[25] J. Cleymans and D. Worku, J. Phys. G **39**, 025006 (2012).
[26] G. Gervino, A. Lavagno, and D. Pigato, Open Phys. **10**, 594 (2012).
[27] A. P. Santos, F. I. M. Pereira, R. Silva, and J. S. Alcaniz, J. Phys. G **41**, 055105 (2014).
[28] V. Khachatryan, A. M. Sirunyan *et al.*, J. High Energy Phys. 02 (2010) 041.
[29] G. Aad, B. Abbott, J. Abdallah *et al.*, New J. Phys. **13**, 053033 (2011).
[30] D. d'Enterria, R. Engel, T. Pierog, S. Ostapchenko, and K. Werner, Astropart. Phys. **35**, 98 (2011).
[31] J. Cleymans, G. Lykasov, A. Parvan, A. Sorin, O. Teryaev, and D. Worku, Phys. Lett. B **723**, 351 (2013).
[32] J. Cleymans, M. D. Azmi, A. S. Parvan, and O. V. Teryaev, EPJ Web Conf. **137**, 11004 (2017).
[33] A. Deppman, E. Megías, and D. P. Menezes, Nucl. Part. Phys. Proc. **312–317**, 166 (2021).
[34] J. Tao, W. Wu, M. Wang, H. Zheng, W. Zhang, L. Zhu, and A. Bonasera, Particles **5**, 146 (2022).
[35] J. I. Cabrillo Bartolomé, A. Calderón Tazón, S. Chuang *et al.*, J. High Energy Phys. 02 (2010) 041.
[36] V. Khachatryan, A. M. Sirunyan, M. Tumasyan *et al.* (CMS Collaboration), Phys. Rev. Lett. **105**, 211801 (2010).
[37] K. Aamodt, N. Abel, U. Abeysekara, A. Abrahantes Quintana, A. Abramyan, D. Adamová, M. Aggarwal, G. Aglieri Rinella, A. Agocs *et al.* (ALICE Collaboration), Eur. Phys. J. C **71**, 1655 (2011).
[38] C. Aguiar and T. Kodama, Physica (Amsterdam) **320A**, 371 (2003).
[39] A. Giovannini and L. Van Hove, Z. Phys. C **30**, 391 (1986).
[40] M. Markytan, W. Majerotto, and J. Macnaughton, eds., *Multiparticle Dynamics Proceedings, 17th International Symposium, Seewinkel, Austria, 1986* (World Scientific Publishing, Singapore, 1987).
[41] G. Alner *et al.*, Phys. Lett. **167B**, 476 (1986).
[42] M. Derrick *et al.*, Phys. Lett. **168B**, 299 (1986).
[43] G. J. Alner *et al.* (UA5 Collaboration), Phys. Rep. **154**, 247 (1987).
[44] J. D. Ramshaw, J. Phys. A **53**, 095003 (2020).
[45] G. D. Yen, M. I. Gorenstein, W. Greiner, and S. N. Yang, Phys. Rev. C **56**, 2210 (1997).
[46] P. Braun-Munzinger, I. Heppe, and J. Stachel, Phys. Lett. B **465**, 15 (1999).
[47] R. G. Mortimer, *Physical Chemistry* (Academic Press, New York, 2000).
[48] D. Oliinychenko, K. Bugaev, and A. Sorin, Ukranian J. Phys. **58**, 211 (2013).
[49] R. E. Ansorge *et al.* (UA5 Collaboration), Z. Phys. C **43**, 357 (1989).
[50] I. Abt, T. Ahmed *et al.*, Nucl. Instrum. Methods Phys. Res., Sect. A **386**, 310 (1997).
[51] A. Breakstone, C. Buchanan *et al.*, Phys. Lett. **135B**, 505 (1984).
[52] W. Bell *et al.*, Nucl. Instrum. Methods **124**, 437 (1975).
[53] A. Breakstone, R. Campanini *et al.* (Ames-Bologna-CERN-Dortmund-Heidelberg-Warsaw Collaboration), Phys. Rev. D **30**, 528 (1984).
[54] P. Virtanen, R. Gommers *et al.*, Nat. Methods **17**, 261 (2020).
[55] S. Aid *et al.* (H1 Collaboration), Z. Phys. C **72**, 573 (1996).